Please cite this article in press as: Srivas et al., A UV-Induced Genetic Network Links the RSC Complex to Nucleotide Excision Repair and Shows Dose-Dependent Rewiring, Cell Reports (2013), http://dx.doi.org/10.1016/j.celrep.2013.11.035

Cell Reports
Resource

A UV-Induced Genetic Network Links the RSC Complex to Nucleotide Excision Repair and Shows Dose-Dependent Rewiring

Rohith Srivas,[1,6] Thomas Costelloe,[2,6] Anne-Ruxandra Carvunis,[1] Sovan Sarkar,[3] Erik Malta,[2] Su Ming Sun,[2] Marijke Pool,[2] Katherine Licon,[1,5] Tibor van Welsem,[4] Fred van Leeuwen,[4] Peter J. McHugh,[3] Haico van Attikum,[2,*] and Trey Ideker[1,5,*]

[1]Department of Medicine, University of California, San Diego, La Jolla, CA 92037, USA
[2]Department of Toxicogenetics, Leiden University Medical Center, Einthovenweg 20, 2333 ZC Leiden, the Netherlands
[3]Department of Oncology, Weatherall Institute of Molecular Medicine, John Radcliffe Hospital, University of Oxford, Oxford OX3 9DS, UK
[4]Division of Gene Regulation, Netherlands Cancer Institute, 1066 CX Amsterdam, the Netherlands
[5]Institute for Genomic Medicine, University of California, San Diego, La Jolla, CA 92037, USA
[6]These authors contributed equally to this work
*Correspondence: h.van.attikum@lumc.nl (H.v.A.), tideker@ucsd.edu (T.I.)
http://dx.doi.org/10.1016/j.celrep.2013.11.035

SUMMARY

Efficient repair of UV-induced DNA damage requires the precise coordination of nucleotide excision repair (NER) with numerous other biological processes. To map this crosstalk, we generated a differential genetic interaction map centered on quantitative growth measurements of >45,000 double mutants before and after different doses of UV radiation. Integration of genetic data with physical interaction networks identified a global map of 89 UV-induced functional interactions among 62 protein complexes, including a number of links between the RSC complex and several NER factors. We show that RSC is recruited to both silenced and transcribed loci following UV damage where it facilitates efficient repair by promoting nucleosome remodeling. Finally, a comparison of the response to high versus low levels of UV shows that the degree of genetic rewiring correlates with dose of UV and reveals a network of dose-specific interactions. This study makes available a large resource of UV-induced interactions, and it illustrates a methodology for identifying dose-dependent interactions based on quantitative shifts in genetic networks.

INTRODUCTION

Helix-distorting DNA lesions, such as those caused by exposure to UV radiation, are sensed and repaired by the nucleotide excision repair (NER) pathway (Prakash and Prakash, 2000). Following damage recognition, the lesion is excised, the resulting gap is filled in by a DNA polymerase, and finally the remaining nick is sealed by a DNA ligase (Prakash and Prakash, 2000). The NER machinery, however, does not work in isolation. Increasing evidence points to the precise coordination of NER with several other biological processes, such as the cell-cycle checkpoint (Sertic et al., 2012) and chromatin remodeling (Gong et al., 2006; Luijsterburg et al., 2012; Sarkar et al., 2010; Yu et al., 2005). Thus, a critical next step in defining the UV damage response will require an understanding of how distinct cellular processes cooperate with NER to promote the efficient repair of UV-induced lesions.

Large-scale screens for genetic interactions, facilitated by high-throughput techniques, such as synthetic genetic arrays (SGA) or diploid synthetic lethal analysis by microarray, have been used with great success to rapidly map functional synergies among most genes in the yeast genome (Costanzo et al., 2010; Pan et al., 2007; Schuldiner et al., 2005, 2006). However, it has become increasingly clear that many gene functional relationships are condition-dependent (St Onge et al., 2007) and identifying genetic networks that are essential to responding to an external stimulus will require a differential methodology. To this end, we have recently developed an interaction-mapping technique termed differential epistasis mapping (Bandyopadhyay et al., 2010) which enables the detection of quantitative changes in genetic interaction following an environmental change. Such differential genetic interactions have been shown to specifically highlight functional connections relevant to stress conditions with both high power and sensitivity (Guénolé et al., 2013).

Toward the goal of defining the crosstalk between NER and other cellular processes following UV irradiation, we constructed a large differential epistasis network by measuring changes in genetic interactions in response to two doses of UV. The genetic data reveal a link between the NER machinery and the *r*emodel the structure of *c*hromatin (RSC) chromatin-remodeling complex. We find that, unlike chromatin-remodeling complexes previously implicated in NER (Gong et al., 2006; Sarkar et al.,

Please cite this article in press as: Srivas et al., A UV-Induced Genetic Network Links the RSC Complex to Nucleotide Excision Repair and Shows Dose-Dependent Rewiring, Cell Reports (2013), http://dx.doi.org/10.1016/j.celrep.2013.11.035

Cell PRESS
Open ACCESS

2010), RSC is recruited to sites of UV-induced lesions in both silenced and transcribed loci, where it helps to promote efficient repair. Finally, we leverage measurements made across multiple doses of UV to pinpoint a network of 79 dose-specific interactions, which, strikingly, are observed only at low or high doses, but not both. This study makes available a large resource of UV-induced differential interactions, which we expect will prove indispensable for modeling the response to UV at the level of single genes, protein complexes, and global processes.

RESULTS

A UV-Based Differential Genetic Interaction Map

To map the functional connections between genes and pathways that underlie the response to UV-induced DNA damage, we measured changes in genetic interactions between a set of 37 query genes (Table S1) and 1,397 array genes (Table S2). Query genes were chosen to represent a majority of the core NER factors and many known chromatin-remodeling complexes, whereas array genes were drawn from numerous functional categories. Using SGA technology (Tong and Boone, 2006), >45,000 double mutant combinations were generated and growth rates were measured in untreated (UT) conditions as well as in response to two doses of UV radiation: a "low" dose of 20 J/m^2 and a "high" dose of 80 J/m^2 (Experimental Procedures; Figure 1A).

Measurements were first analyzed to assign each double mutant a "static" interaction score in each condition separately (S_{UT}, S_{Low}, and S_{High}) which reflects the extent to which the double mutant either grew better ($S > 0$; positive interaction or epistasis) or worse than expected ($S < 0$; negative interaction or synthetic sick). To assess shifts in interaction following UV irradiation, the difference in static scores between treated and untreated conditions ($S_{Low} - S_{UT}$ and $S_{High} - S_{UT}$) was computed for each gene pair and then assigned a p value ($P_{High\ -\ UT}$, $P_{Low\ -\ UT}$) using a null distribution of differences observed when comparing replicate measurements made in the same condition (Experimental Procedures). Using previously established static ($S \geq 2.0$ or $S \leq -2.5$; Experimental Procedures) or differential interaction thresholds ($P_{High\ -\ UT}$, $P_{Low\ -\ UT} \leq 0.001$; false discovery rate [FDR] $\approx$ 7%; see Figure S1A), we thus obtained three static genetic networks and two differential genetic networks (Figure 1A; Table S3 for raw data). Quality control metrics were monitored through this process, ensuring the high quality of these data sets (Figures S1B–S1D).

All three static networks were enriched for interactions involving genes that function in chromatin organization, as has been noted previously for other genetic interaction data (Bandyopadhyay et al., 2010; Guénolé et al., 2013). In contrast, the two differential networks exhibited no such enrichment (Figure 1B), as strong signals present in both conditions are effectively "cancelled out" in the differential mode of analysis (Ideker and Krogan, 2012). Instead, the two differential networks were highly enriched for interactions involving genes functioning specifically in the NER pathway (Figure 1B). In addition, we found that the number of differential interactions per gene (Figures 1C and S1E), as well as the extent to which a gene's static interaction profile was disrupted by UV treatment, is correlated with the UV sensitivity of the corresponding gene deletion strain (Figures 1D and S1F). The static and differential networks thus provide complementary maps of cellular organization, with the differential networks highlighting genes most relevant to the UV damage response.

Differential Genetic Data Link the RSC Complex to NER

To identify genes and pathways operating in the UV damage response, we integrated all of our genetic data with existing protein-protein interaction data to construct a global map of gene modules and their UV-induced differential interactions. Past work has indicated that sets of genes enriched for static genetic and physical interactions (i.e., modules) often encode for components of the same pathway or complex (Bandyopadhyay et al., 2008; Srivas et al., 2011). On the other hand, differential genetic interactions tend to occur between genes belonging to distinct complexes and represent UV-induced crosstalk or synergy between the two complexes (Bandyopadhyay et al., 2010). Using a previously described workflow (Srivas et al., 2011), we organized our data into a set of 89 functional interactions among 62 modules (Figure 2A; Tables S4 and S5; Experimental Procedures).

Detailed inspection of this module map both recapitulates current understanding and suggests many hypotheses. For example, we observed a link between Rad6p/Rad18p and the translesion synthesis polymerase Polζ. This is consistent with past work which has shown that monoubiquitination of proliferating cell nuclear antigen by the Rad6p-Rad18p dimer leads to the direct activation of Polζ-dependent bypass of DNA lesions through translesion synthesis (Prakash et al., 2005). We also observed crosstalk between the single-stranded DNA endonuclease Rad1p-Rad10p and the mismatch repair proteins Msh2p/Msh3p/Msh6p; several studies have implicated a joint role for these complexes in ensuring genetic fidelity during mitotic recombination (Saparbaev et al., 1996; Sugawara et al., 1997).

Our map also revealed a significant number of complexes involved in chromatin organization ($p = 0.031$, Fisher's exact test; Figure 2A). This observation was not expected given the lack of enrichment for interactions with genes annotated to this function in the differential networks (Figure 1B), thus suggesting a NER-specific role for these complexes. For example, the INO80 chromatin-remodeling complex was found to interact with the Rad1p-Rad10p dimer, which is consistent with a recent finding that INO80 is required for efficient repair of UV-induced lesions at a heterochromatic locus (Sarkar et al., 2010). Another chromatin-remodeling complex that was featured prominently in our map with links to two different NER modules (Rad4p/Rad23p and Rad1p/Rad10p) was RSC. RSC is a highly conserved chromatin-remodeling complex with DNA-dependent adenosine triphosphatase activity (Cairns et al., 1996) but as of yet has no known role in the UV damage response. We observed multiple interactions between components of the RSC complex (Rsc1p, Rsc3p, Rsc58p, and Arp7p) and several NER factors, including Rad1p and Rad4p (Figure 2B) as well as more moderate differential positive interactions between *RSC3* and *RAD14/RAD16* ($p = 0.01$). Moreover, we found that deletion of nonessential genes

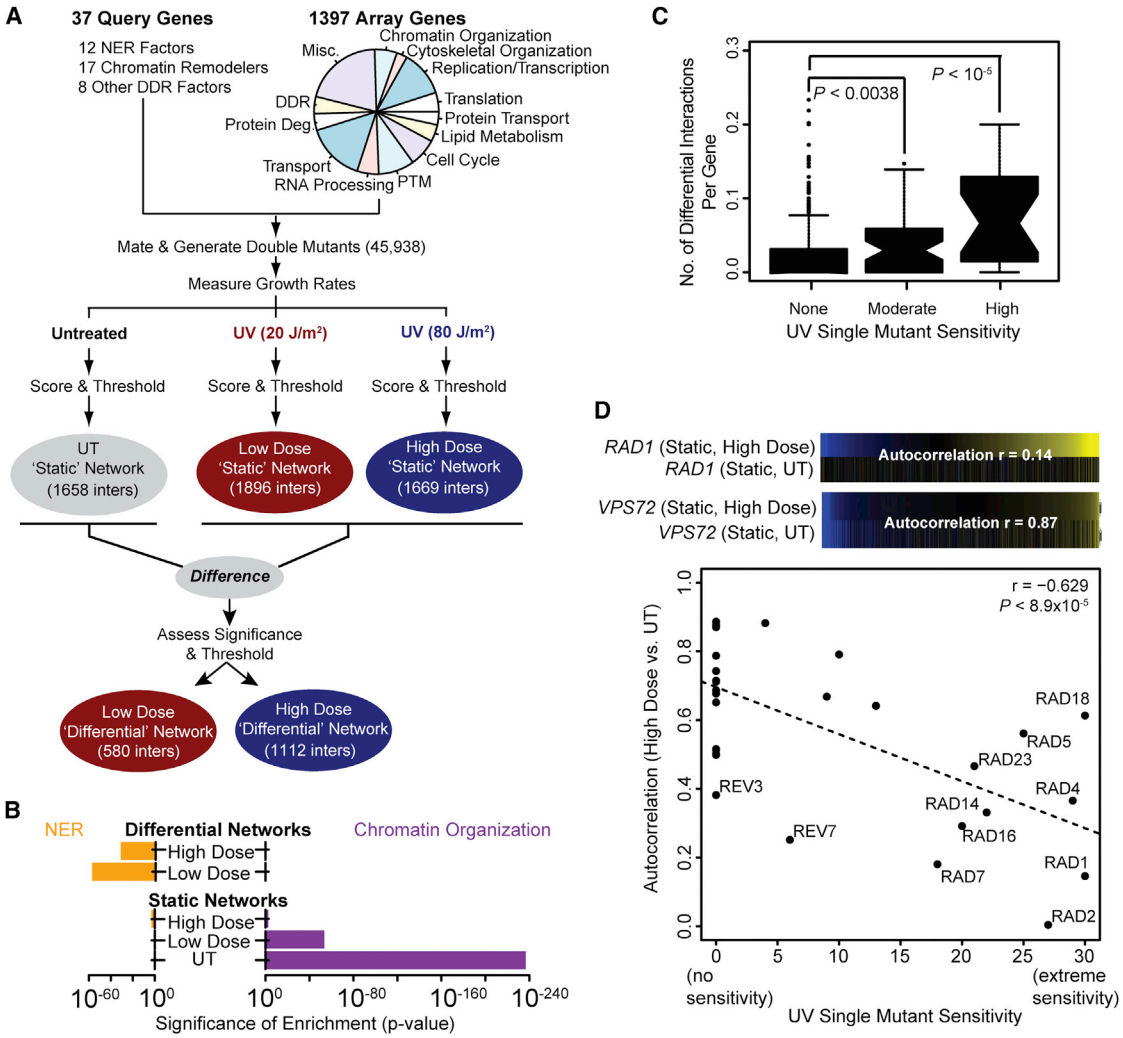

Figure 1. A UV-Induced Differential Genetic Network

(A) Outline of the genetic interaction screen. The functional categories represented by the array genes are shown in the pie chart (misc, miscellaneous; DDR, DNA damage response; protein deg., protein degradation; PTM, posttranslational modifications). See Table S2 for more details.

(B) The significance of enrichment for interactions with genes annotated to nucleotide excision repair (NER) or chromatin organization (see Table S7 for process definitions) is shown for each network. Enrichment p values were calculated as previously described (Bandyopadhyay et al., 2010).

(C) Each gene considered in this study is binned according to its UV-induced single-mutant sensitivity (Begley et al., 2004) and the distribution of the number of high-dose differential interactions for all genes in a bin (number of significant differential interactions/number of tested differential interactions) is summarized as a box-and-whisker plot. Significance is assessed using a Mann-Whitney U test.

(D) For each query gene, the Pearson's correlation between its high-dose static interaction profile and static untreated profile ("autocorrelation") is plotted against the gene's UV-induced single-mutant sensitivity (Begley et al., 2004). The high-dose and untreated static profiles are shown for two query genes: *RAD1* and *VPS72*. See also Figure S1.

encoding RSC subunits (*RSC2* and *HTL1,* but not *RSC1*; Figures 2C, S2A, and S2B) as well as depletion of RSC subunits encoded by essential genes (*RSC3*, *RSC8*, and *STH1*; Figures 2D and S2A) led to increased UV sensitivity. Together, these observations support the hypothesis that RSC is required during the UV damage response.

Rsc2 Is Required for NER at Both Transcribed and Silenced Loci

The UV sensitivity of RSC-deficient strains could be caused by a checkpoint or NER defect. To distinguish between these possibilities, we first examined checkpoint activation in wild-type (WT) and *rsc2*Δ cells following exposure to UV. Analysis of the phosphorylation levels of Rad53 (a central effector of the checkpoint response) revealed efficient checkpoint activation, with Rad53 becoming phosphorylated within 30 min after UV exposure and remaining phosphorylated for at least 3 hr in both WT and *rsc2Δ* cells (Figure S2C). Furthermore, fluorescence-activated cell sorting (FACS) analysis revealed no major differences in the cell-cycle profile between WT and *rsc2*Δ following UV exposure (Figure S2C), indicating normal checkpoint activation following UV irradiation in *rsc2*Δ cells. A similar phenotype has

Please cite this article in press as: Srivas et al., A UV-Induced Genetic Network Links the RSC Complex to Nucleotide Excision Repair and Shows Dose-Dependent Rewiring, Cell Reports (2013), http://dx.doi.org/10.1016/j.celrep.2013.11.035

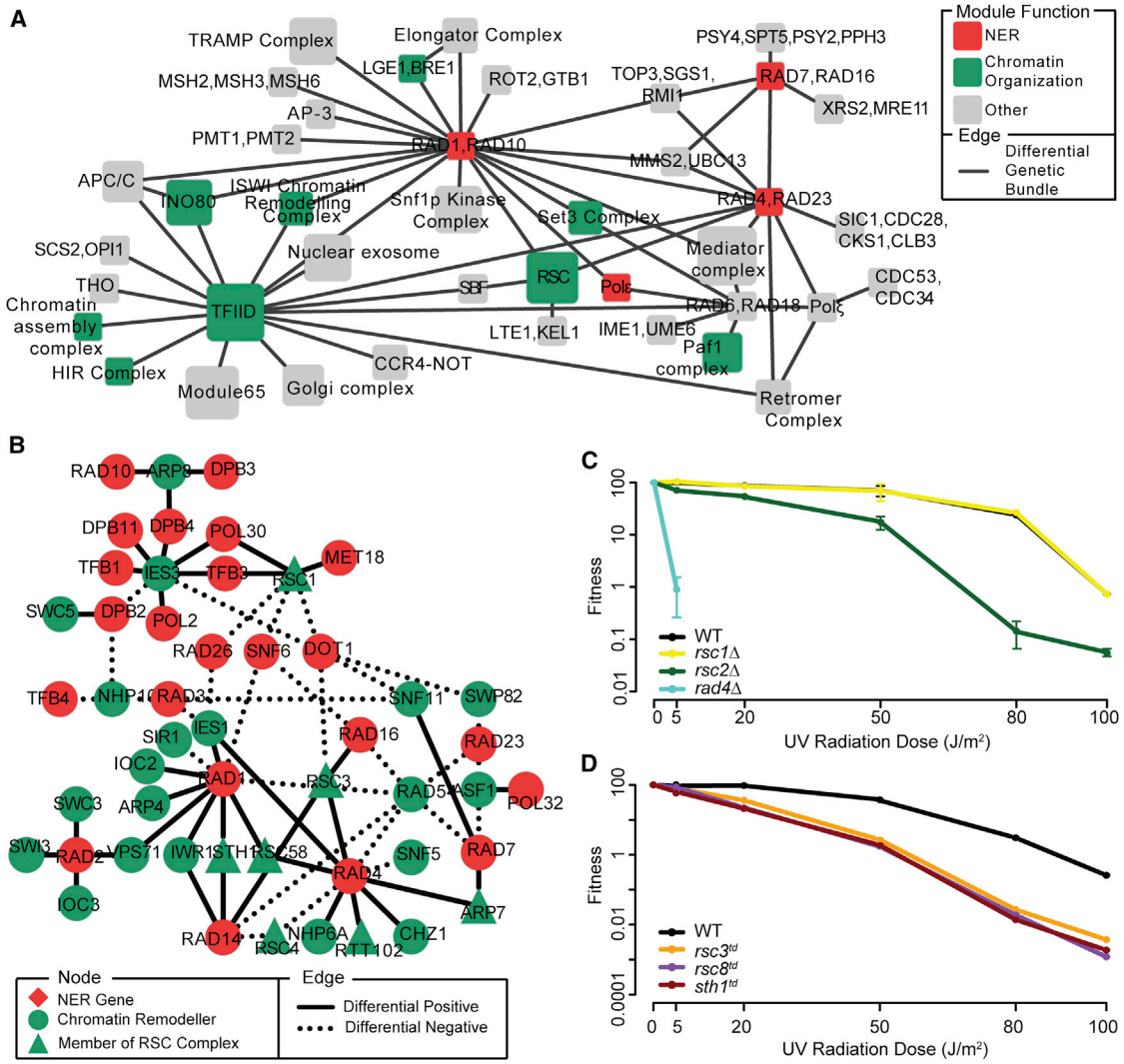

Figure 2. Differential Genetic Data Links RSC to NER

(A) A map of multigenic modules spanned by bundles of UV-induced differential interactions. Node size scales with the number of genes in each module, whereas the node color indicates its function (see Table S7 for a list of process definitions). Modules that overlap with known protein complexes have been labeled accordingly; otherwise, a generic name has been provided. For the sake of clarity, only a portion of the module map has been shown here. See Table S5 for the complete list of module-module interactions.

(B) Differential genetic interactions (P_{Low-UT} or $P_{High-UT} \leq 0.03$) seen between chromatin remodelers and components of the NER pathway (see Table S7 for a list of process definitions).

(C and D) Survival curves for mutants in (C) nonessential or (D) essential genes encoding subunits of RSC following exposure to UV radiation across multiple doses. Survival curves were generated through quantification of the spot dilution assay in Figure S2A and one additional replicate (data not shown). Fitness was calculated by counting the number of colonies present in the most dilute spot containing individual colonies and then dividing the count in UV-treated conditions by the count in untreated conditions. All data represent the mean ± one SEM of two independent replicates. See also Figures S2 and S3.

been noted in *rsc2*Δ mutants following exposure to the DNA alkylating agent, methyl methanesulfonate (Chambers et al., 2012).

To monitor the efficiency of NER in WT and *rsc2*Δ cells, we used a sensitive quantitative PCR (qPCR)-based assay (Experimental Procedures) to measure the rate of repair within the highly transcribed *MATa* locus and the nontranscribed *HMLα* locus. At both loci, UV lesions were rapidly repaired in WT cells (~80% lesions removed by 3 hr; Figures 3A and 3B), whereas the rate of repair in the NER-deficient *rad14Δ* mutants (Guzder et al., 1993) was significantly reduced ($P_{MATa} = 1.1 \times 10^{-5}$ and $P_{HML\alpha} = 1.8 \times 10^{-9}$; F test). The *rsc2Δ* cells, whereas not as deficient in repair as *rad14*Δ cells ($P_{MATa} = 0.024$ and $P_{HML\alpha} = 0.013$; F test), had nearly twice as many lesions present as WT at both loci 3 hr after UV exposure, indicating that RSC contributes to an efficient NER response. Importantly, both WT and *rsc2*Δ cells were found to accumulate equivalent amounts of UV-induced lesions, suggesting that the difference in repair rates is not due to differences in DNA damage susceptibility in these cells (Figure S2D).

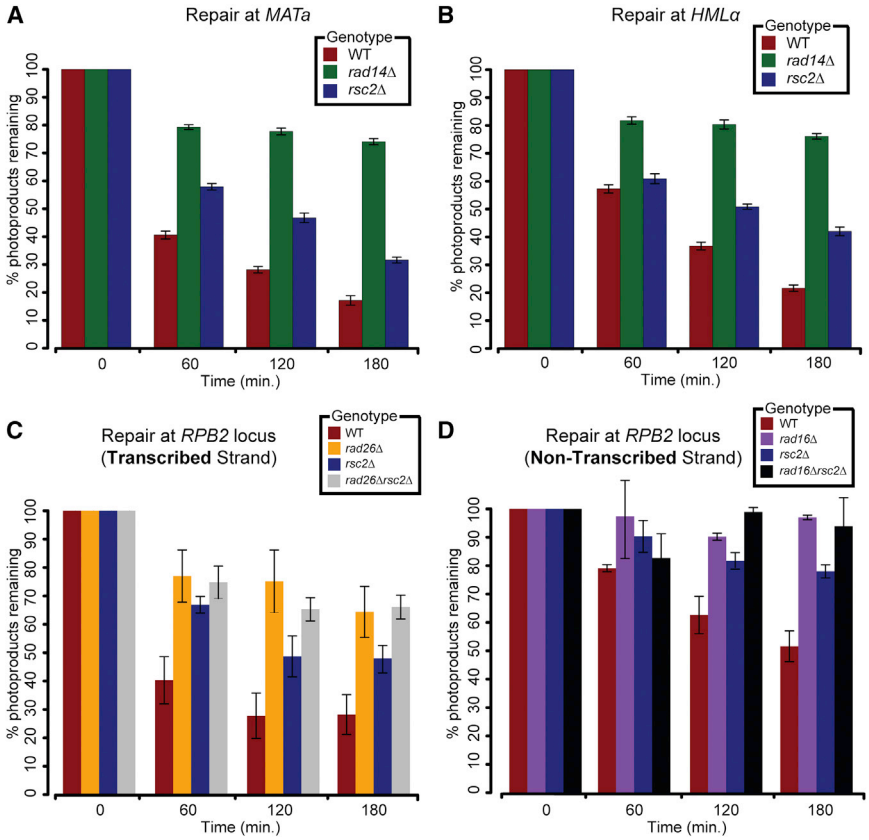

Figure 3. RSC Is Required for Efficient TCR- and GGR-NER

(A and B) Rate of photoproduct removal at the (A) *MATa* and (B) *HMLα* loci measured in G1-synchronized cells using a sensitive qPCR-based assay (Experimental Procedures).

(C and D) Rate of photoproduct removal on the (C) transcribed and (D) nontranscribed strands of the *RPB2* locus measured in G1-synchronized cells using a strand-specific repair assay (Experimental Procedures). All data represent the mean ± one SEM of at least three independent replicates.

NER is composed of two distinct pathways, global genome repair (GGR) and transcription-coupled repair (TCR), which remove, respectively, lesions throughout the entire genome or on the transcribed strand of expressed loci only (Prakash and Prakash, 2000). Whereas both the INO80 and *swi*tch/*s*ucrose *n*onfermentable (SWI/SNF) complexes have been implicated in NER previously, neither was found to have a role in promoting efficient TCR (Gong et al., 2006; Sarkar et al., 2010). Strikingly, deletion of *RSC2* or *STH1* (catalytic core of the RSC complex) in combination with either *RAD26* (encoding a component of TCR) or *RAD16* (encoding a component of GGR) revealed a UV-dependent synthetic sick relationship (Figures S3A–S3G). We also observed a differential negative interaction between *RSC2* and *RAD14* (encoding a component of both GGR and TCR; Figures S3A and S3D). Together with our finding that RSC mediates efficient repair in a variety of genomic contexts (Figures 3A and 3B), these data suggest that RSC may affect both pathways of NER.

To assess RSC's role in both GGR and TCR, we employed an assay in which we measured the rate of photoproduct removal at the nontranscribed and transcribed strands of the *RPB2* locus (Experimental Procedures). Critically, all experiments were performed in G1-arrested cells in which lesion removal is dependent solely on NER (Gong et al., 2006, 2008; Sarkar et al., 2010; Smerdon and Lieberman, 1978) and any effect of DNA replication or replication fork stalling/collapse due to photoproduct induction can be ruled out. As expected, in *rad26*Δ and *rad16*Δ cells in which, respectively, TCR (Aboussekhra and Al-Sharif, 2005) and GGR (Verhage et al., 1994) are completely abrogated, we observed virtually no repair over the duration of the experiment, neither at the transcribed (Figure 3C) nor nontranscribed strands (Figure 3D). In *rsc2Δ* cells, repair at both strands was compromised compared to wild-type, but not completely abolished, with, respectively, ~1.8 and ~1.5 times more photoproducts present at 3 hr after UV irradiation. This suggests that RSC is required, but not essential, for GG- and TC-NER. Finally, the *rsc2*Δ*rad16*Δ and *rsc2*Δ*rad26*Δ double mutants displayed a reduction in the rate of repair similar to that of the corresponding NER-deficient single mutants suggesting a potential epistatic effect and providing further evidence for a role for RSC in both NER pathways. Importantly, the reduced rate of repair seen at the transcribed strand of *RPB2* in *rsc2*Δ cells was not due to transcriptional misregulation, as the expression level of *RPB2* was comparable in WT and *rsc2Δ* cells (Figure S3H).

RSC Is Recruited to Sites of UV Lesions via Rad4 and Promotes Nucleosome Remodeling

We considered that RSC might affect NER indirectly by regulating the expression of one or more NER factors or by acting directly at sites of UV lesions. To test the former hypothesis, we obtained previously published gene expression data generated in RSC mutants in nominal conditions (Lenstra et al., 2011). Analysis of these data found no changes in the expression of NER factors, whereas only nine genes annotated to the broader DNA damage response appeared to be differentially expressed in a RSC mutant compared to wild-type (Figure S4A). However, none of these nine genes were found previously to be differentially expressed following exposure to UV (Wade et al., 2009). Finally, we randomly selected 11 core NER genes and measured their expression levels via qPCR in both wild-type and *rsc2*Δ cells following UV exposure (Experimental Procedures). None of these genes' changes in UV-induced expression were found to be dependent on Rsc2 (Figure S4B). Together, this suggests that Rsc2 does not affect NER indirectly through transcriptional regulation of NER factors.

Please cite this article in press as: Srivas et al., A UV-Induced Genetic Network Links the RSC Complex to Nucleotide Excision Repair and Shows Dose-Dependent Rewiring, Cell Reports (2013), http://dx.doi.org/10.1016/j.celrep.2013.11.035

Cell PRESS
Open ACCESS

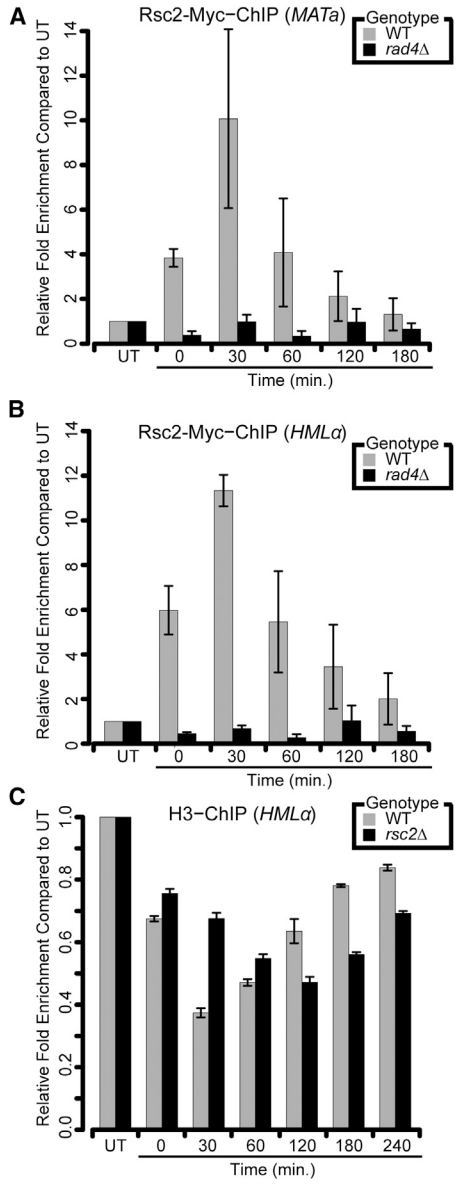

Figure 4. RSC Promotes Proper Nucleosome Remodeling following UV-Induced Damage

(A and B) Analysis of Rsc2-Myc recruitment to either (A) *MATa* or (B) *HMLα* following exposure to UV radiation.

(C) Analysis of histone H3 occupancy at the *HMLα* locus following UV exposure in G1-synchronized cells. All data represent the mean ± one SEM of at least three independent replicates. See also Figure S4.

We next asked if RSC might be acting directly at UV lesions. Using a modified chromatin immunoprecipitation (ChIP) protocol that allows the analysis of protein occupancy in the presence of UV photoproducts (Experimental Procedures; Sarkar et al., 2010), we monitored Rsc2-Myc recruitment to *MATa* and *HMLα* following UV irradiation (Figures 4A and 4B). In wild-type cells, Rsc2-Myc accumulates at both loci almost immediately after irradiation, reaches maximal occupancy at 30 min postirradiation, and then decreases during the remainder of the experiment. Rsc2 recruitment was UV damage-dependent as we observed little enrichment of Rsc2-Myc at either locus in untreated conditions (Figure S4C). Finally, we also observed strong recruitment of Sth1-Myc to both loci in a UV-dependent fashion, providing further evidence for the recruitment of the RSC complex to damaged chromatin (Figure S4D).

Rad4 is a core NER factor responsible for the initial damage recognition step and subsequent recruitment of other NER factors (Jansen et al., 1998). Previous work has shown an important role for Rad4 in mediating the recruitment of chromatin remodelers to sites of UV-induced lesions (Gong et al., 2006; Sarkar et al., 2010). Thus, we asked whether Rad4 may play a similar role in targeting RSC to damaged chromatin. Using our modified ChIP assay, we observed that Rad4-Myc was recruited to both loci in a UV-dependent manner (Figure S4D), indicating that both Rad4 and RSC are present at the same sites of UV damage. Moreover, deletion of *RAD4* completely abrogated Rsc2-Myc accumulation at both loci (Figures 4A and 4B). Together, these results suggest that Rad4 is required for the recruitment of RSC to sites of UV damage.

RSC possesses the capability to perturb nucleosome structures (Cairns et al., 1996, 1999; Saha et al., 2002), suggesting that it may affect nucleosome remodeling dynamics at UV lesions to promote NER. To test this hypothesis, we monitored levels of histone H3 at the *HMLα* locus following UV treatment. In the WT strain, we observed a rapid loss of histone H3 within the first 30 min, followed by a gradual restoration over the next 3 hr (Figure 4C). These results are consistent with the rates of repair seen earlier (Figure 3), in which the majority of repair occurs within the first hour and is completed within 3 hr. In *rsc2Δ* mutants, we observed a delay in both the initial loss of H3 around UV lesions, as well as restoration of H3 occupancy at later time points (Figure 4C). As there was minimal difference in histone H3 levels between WT and *rsc2Δ* in untreated conditions, these results suggest that RSC promotes proper nucleosome remodeling at sites of UV lesions (Figure S4E).

Comparing Network Rewiring across Low and High Levels of UV

As this study measures genetic interactions in response to varying doses of the same agent, we next compared the effect of low versus high UV dose on the genetic network. We found that both UV-induced differential genetic networks had significant similarity, especially in comparison to networks measured under genotoxic agents other than UV (Figures 5A and S5A). On the other hand, the high dose induced nearly twice the number of genetic interaction changes than the low dose (1,112 versus 580; Figure 5A). This observation was clear through analysis of either differential (Figure 5A) or static networks (Figure S5B) and was robust to the choice of threshold used to define significant interactions (Figures S5C and S5D). Thus, whereas both UV doses produce overlapping networks and highlight gene functions related to the NER pathway, they also appear to induce a network of dose-specific interactions.

To further characterize this space of potential dose-specific interactions, we visualized the underlying static genetic changes between untreated, low-dose, and high-dose conditions for each of these interactions (Figures 5B). Visualizing the data in

Cell PRESS
Open ACCESS

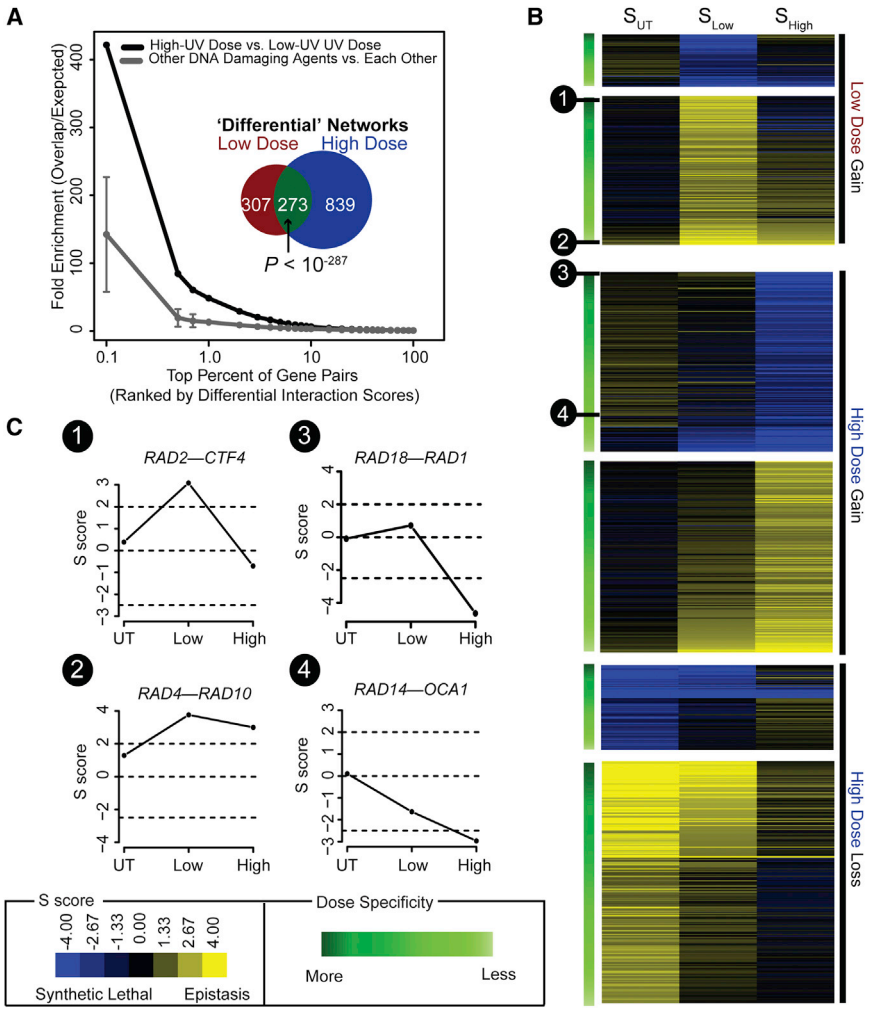

Figure 5. Identifying Dose-Specific Differential Interactions

(A) Overlap between high-UV and low-UV dose differential networks (black line) or the average overlap seen among three previously published differential networks generated in response to distinct genotoxic agents (dark gray line/"Other DNA-Damaging Agents"; Guénolé et al., 2013). Fold enrichment is defined as n/r, where n is the number of top-ranked gene pairs (x axis; ranked by differential p value) common to a pair of networks and r is the number expected at random. Error bars indicate one SD. The inset shows the overlap between all significant differential interactions ($P_{Low\ -\ UT}$, $P_{High\ -\ UT} \leq 0.001$) uncovered in high-dose versus low-dose conditions. Significance of overlap was assessed using a one-tailed Fisher's exact test.

(B) Heat map of the static dose profiles ($S_{UT} \rightarrow S_{Low} \rightarrow S_{High}$) for all 849 and 307 high- and low-dose differential interactions. Interactions have been categorized as "gain of interaction" or "loss of interaction" and then ordered (top to bottom) based on their likelihood of being a dose-specific differential interaction. For more details, see Supplemental Experimental Procedures.

(C) Example static dose profiles are shown for four interactions. See also Figure S5.

this manner revealed a continuum of differential interactions ranging from those interactions which displayed a marked change in interaction exclusively in low or high UV dose compared to untreated (e.g., *RAD2-CTF4* and *RAD18-RAD1*; Figure 5C) to interactions in which a shift in genetic interaction was observed at both UV doses compared to untreated, but where the magnitude of this shift differed between doses (e.g., *RAD4-RAD10* and *RAD14-OCA1*; Figure 5C).

To explicitly identify dose-specific interactions, i.e., interactions with a strong change in one dose only, we developed a bioinformatics pipeline to analyze an interaction's underlying static dose profile. As described further in the Supplemental Experimental Procedures, we first defined a set of model dose profiles representing high- or low-dose-specific interactions (Figure S5E), as well as a "null" model profile devoid of change between UV doses. Interactions whose static dose profile more closely aligns with a dose-specific profile compared to the null model are classified as dose-specific interactions. Applied to our data set, our method identified, respectively, 35 and 44 high- and low-dose-specific interactions (Table S6; FDR < 40%).

These dose-specific connections were enriched for interactions with genes annotated to DNA metabolism (p = 0.00012; high dose), DNA recombination (p = 0.00012; high dose), translesion synthesis (p = 0.02459; low dose), and intriguingly protein degradation (p = 0.0146; low dose). Consistent with these observations, exposure to genotoxic agents, including UV radiation, has previously been shown to result in increased rates of protein degradation (Burgis and Samson, 2007). Strikingly, we found that all low-dose-specific interactions involved NER genes involved in downstream repair activities, such as DNA incision and gap filling (*RAD1*, *RAD2*, and *RAD10*), and not by any of the early sensors. Consistent with this observation, deletion of factors involved in sensing DNA damage was found to have no impact on the rate of damage-induced protein degradation (Burgis and Samson, 2007), suggesting that the signal for increased protein degradation does not originate from the damaged DNA itself.

Although further work will be required to resolve the precise mechanisms underlying these dose-specific connections, our study provides an important proof of principle that the framework for analyzing shifts in genetic networks in response to external stimuli (Bandyopadhyay et al., 2010; Bean and Ideker, 2012) can be expanded to understand how such networks are influenced by varying dosage.

DISCUSSION

Here, we have mapped the UV-induced genetic network between most components of the NER pathway and over 1,300 genes spanning a wide range of biological processes

(Figure 1A). Unlike previous differential genetic studies (Bandyopadhyay et al., 2010; Guénolé et al., 2013), we have made measurements across multiple doses of treatment and developed a bioinformatics pipeline to specifically identify dose-specific interactions (Figure 5; Supplemental Experimental Procedures). Whereas the induction of genetic interactions exclusively at higher doses may be expected, our data also implicate a number of low-dose-specific connections (Table S6), suggesting the presence of response pathways unique to low versus high doses of DNA damage. Indeed, past genome-wide expression studies have shown the induction of transcriptional programs at low (but not high) concentrations of other genotoxic agents, such as methyl methanesulfonate (MMS) and ionizing radiation (Benton et al., 2006). Future studies may combine differential genetic interaction mapping with our bioinformatics pipeline to the study of other genotoxic agents that have known shifts in the mode of action between high and low doses. For example, moderate to high doses of hydroxyurea inhibit DNA, RNA, and protein synthesis, whereas at low concentrations, it interferes exclusively with DNA synthesis (Timson, 1969). Similarly, low concentrations of MMS have been shown to activate only the intra-S checkpoint, whereas higher doses also lead to activation of the G1/S checkpoint (Frei and Gasser, 2000). Examining dose-specific genetic networks may help to disentangle the pathways contributing to the distinct modes of action of these compounds.

Combining our differential genetic data with other physical interaction data sets (Collins et al., 2007; Gavin et al., 2006; Krogan et al., 2006) revealed a link between the RSC chromatin-remodeling complex and both pathways of NER, making RSC the first complex to be linked to TCR (Figures 2B, 3, and S3A–S3G). We found that Rsc2 is recruited in a UV-dependent manner to both expressed and silenced loci (Figures 4A and 4B) and that deletion of *RSC2* led to altered histone-remodeling dynamics at sites of UV damage (Figure 4C). It is worth noting that the remodeling defect observed in *rsc2Δ* cells is not as severe as that observed in *rad4Δ* cells, possibly due to the fact that other chromatin remodelers, such as INO80, are also recruited to sites of UV damage in a Rad4-dependent manner (Gong et al., 2006; Sarkar et al., 2010). Whereas Sth1 (and not Rsc2) forms the catalytic core of the RSC complex, in vitro studies have demonstrated that purified Sth1, without other RSC components (including Rsc2), exhibits a severe reduction in remodeling activity (Saha et al., 2002). These results, coupled with our data showing recruitment of Sth1 and Rsc2 to sites of UV-induced lesions (Figure S4D), lead us to conclude that RSC mediates efficient NER by remodeling chromatin at sites of UV damage.

How might RSC be recruited to damaged chromatin? One possibility is that NER factors, such as Rad4, Rad23, or Rad26, which are responsible for initial damage recognition (Prakash and Prakash, 2000), may physically interact with RSC to facilitate its recruitment. Although we were not able to demonstrate a physical interaction between Rsc2 and Rad4 or Rad23 (data not shown), the RSC complex contains over 15 different subunits (as defined in the *Saccharomyces* Genome Database) and thus an interaction with these NER factors might also occur through one of the other subunits. Alternatively, the damage recognition step itself may help to recruit RSC to chromatin. Structural studies of Rad4-DNA complexes have shown that the binding of Rad4 at UV-induced lesions results in the destabilization of the helical structure (Min and Pavletich, 2007) and the formation of a highly kinked structure (Janićijević et al., 2003). Such structures have been shown to act as a platform for the assembly of an active NER complex, and it is tempting to speculate that they may also serve to promote the recruitment of RSC to damaged chromatin.

Acetylation of histone H3 lysine 14 (H3K14) by NER factors Gcn5 and Rad16 is a critical mark for efficient NER (Teng et al., 2002). Past work has shown that Rsc4, one of the RSC subunits, contains a tandem bromodomain that binds specifically to H3K14ac (VanDemark et al., 2007). Moreover, Rsc4 itself is known to be acetylated by Gcn5, an event which has been shown to be important for promoting resistance to DNA damage and replicative stress (Charles et al., 2011). This suggests that posttranslational modification of either histones or components of RSC may also contribute to the recruitment and regulation of RSC-dependent chromatin remodeling at sites of UV-induced lesions.

Rsc1 and Rsc2 are known to define two mutually exclusive RSC complexes (Cairns et al., 1999) and appear to have overlapping, but not identical, functions (Cairns et al., 1999; Hillenmeyer et al., 2008; Rossio et al., 2010). For example, whereas both mutants are sensitive to double-stranded break-inducing agents and exhibit defects in nonhomologous end joining, these defects could not be rescued by additional copies of the other gene, suggesting similar, but nonoverlapping, functions (Chai et al., 2005; Chambers et al., 2012; Kent et al., 2007). Here, we found that deletion of *RSC2*, but not *RSC1*, rendered cells sensitive to UV (Figure 2C). Consistent with this finding, recent work has implicated a role for Rsc2, but not Rsc1, in the replication of UV-damaged DNA (Niimi et al., 2012). However, given that our differential network revealed several connections between *RSC1* and DNA damage response factors, we cannot exclude a role for the Rsc1-containing complex in the UV response. For instance, Rsc1 may function in other facets of the UV damage response, such as facilitating the repair of DNA breaks that arise as a consequence of UV-induced replication fork collapse.

To facilitate access to our resource, we have made all data available as Cytoscape session files on a supplemental website (http://chianti.ucsd.edu/~rsrivas/srivas_2013/). Using Cytoscape (Shannon et al., 2003), one can query for genes of interest and easily browse the higher-level analysis of interactions between complexes (Figure 2A). Data on UV single-mutant sensitivity, as well as gene-level data from the *Saccharomyces* Genome Database (Cherry et al., 2012), have been added to the session files, allowing for a wealth of information from different fields to be cross-referenced. We anticipate that this resource will be invaluable in increasing our understanding of the UV damage response.

EXPERIMENTAL PROCEDURES

Differential Genetic Experiments

Double mutants were constructed using the SGA technology (Tong and Boone, 2006), except that, in the final step, double mutants were

replica-pinned on the prescribed media and exposed to UV-C radiation (20 J/m^2 and 80 J/m^2) or mock treatment. Static and differential scores were computed as previously described (Bandyopadhyay et al., 2010; Collins et al., 2006). A list of all strains used is provided in Table S8.

Constructing the Module Map

A list of multigenic modules was obtained from a previous study (Guénolé et al., 2013). This list was filtered to include only those modules that contained at least two genes for which we had screened genetic interactions resulting in a list of 123 modules. The sum of the absolute value of differential scores for gene pairs spanning two modules was then compared to a null distribution of summed differential scores for equal-sized random samples of gene pairs. This analysis was performed separately for low-dose and high-dose differential networks, after which a threshold of $p < 0.012$ was used to generate the module map (Figure 2A; Tables S4 and S5).

Transcription Analysis

Mid-log-phase cultures of cells were exposed to UV-C radiation (100 J/m^2) or mock treatment and allowed to recover in yeast extract; peptone; dextrose (YPD) media for 60 min at 30°C. Cells were then lysed, and RT-qPCR was performed as previously described (Chen et al., 2013). For a list of primers used, see Table S9. Measurements were normalized against the housekeeping gene *GCN4*, and final fold changes were computed using the Pfaffl method (Pfaffl, 2001).

Repair Assays

Photoproduct removal rates at *MATa, HML*α, and *RPB2* were determined as described previously (den Dulk et al., 2006; Sarkar et al., 2010). To test for a difference in the rate of photoproduct removal between two strains, a standard linear model was built in which "% photoproducts remaining" was regressed against factors "time," "strain" (categorical variable representing the genotype of the strain, e.g., WT or *rsc2*Δ), and an interaction term (time * strain). The significance of the interaction term, which represents the difference in the rate of photoproduct removal between strains, was then assessed using an F test. All statistical analysis was performed in R (version 2.11.1).

Cell-Cycle-Profiling Experiments

Exponentially growing cells were exposed to UV (70 J/m^2) and then released into fresh YPD medium. FACS analysis was performed at different time points following UV irradiation using a BD LSRII instrument and WinMDI software. Rad53 phosphorylation status was monitored via western blot analysis using a Rad53 antibody (Santa Cruz Biotechnology) as previously described (Guénolé et al., 2013).

Measuring Protein Occupancy at UV-Induced Lesions by ChIP-qPCR

ChIP-qPCR experiments were performed as described previously (Sarkar et al., 2010) using either an antibody against histone H3 (Abcam number AB1791) or Myc (Cell Signaling Technology number 9B11). Briefly, cells were exposed to UV radiation (200 J/m^2) and harvested at the indicated time points (Figure 4). Cells were then processed as for conventional ChIP, except that after immunoprecipitation (IP) and reversal of DNA-protein cross-links, the DNA was treated with 5 μg *D. melanogaster* 6-4 photolyase and 50 ng *Escherichia coli* cyclobutane pyrimidine dimer photolyase for 1 hr at room temperature to remove all unrepaired UV lesions and permit equal amplification of all DNA. In addition, an aliquot of each extract was taken prior to immunoprecipitation and treated with photolyase enzymes ("input"), and a no antibody control IP was performed ("no antibody"). IP, input, and no antibody DNA were subsequently analyzed by RT-qPCR using primers targeting *MATa* or *HML*α (see Table S9 for primer sequences). Absolute enrichment for histone H3, Rsc2, Sth1, or Rad4 at these loci was calculated by comparing IP threshold cycle values (C_t) to no antibody values using input as a reference. Finally, relative fold enrichment was defined as the ratio of absolute enrichment of UV-treated samples to that of untreated samples (UT).

Additional experimental details have been provided in the Supplemental Experimental Procedures.

SUPPLEMENTAL INFORMATION

Supplemental Information includes Supplemental Experimental Procedures, five figures, and nine tables and can be found with this article online at http://dx.doi.org/10.1016/j.celrep.2013.11.035.

ACKNOWLEDGMENTS

The authors thank C. Logie for generously providing yeast strains; L. Mullenders for providing the opportunity to perform the screen; A. Guénolé and I. Stulemeijer for assistance with the screen; P. Jaeger, G. Hannum, G. Bean, and M. Hofree for insightful discussions; and J.P. Shen for a critical reading of the manuscript. This work was supported by grants from the U.S. National Institutes of Health to T.I. (ES014811 and GM084279), the Netherlands Organization for Scientific Research (NWO-VIDI and TOP-GO) and Human Frontiers Science Program (CDA grant) to H.v.A., and a Programme Grant from Cancer Research (UK) to S.S. and P.J.M.

Received: May 4, 2013
Revised: October 5, 2013
Accepted: November 20, 2013
Published: December 19, 2013

REFERENCES

Aboussekhra, A., and Al-Sharif, I.S. (2005). Homologous recombination is involved in transcription-coupled repair of UV damage in Saccharomyces cerevisiae. EMBO J. *24*, 1999–2010.

Bandyopadhyay, S., Kelley, R., Krogan, N.J., and Ideker, T. (2008). Functional maps of protein complexes from quantitative genetic interaction data. PLoS Comput. Biol. *4*, e1000065.

Bandyopadhyay, S., Mehta, M., Kuo, D., Sung, M.K., Chuang, R., Jaehnig, E.J., Bodenmiller, B., Licon, K., Copeland, W., Shales, M., et al. (2010). Rewiring of genetic networks in response to DNA damage. Science *330*, 1385–1389.

Bean, G.J., and Ideker, T. (2012). Differential analysis of high-throughput quantitative genetic interaction data. Genome Biol. *13*, R123.

Begley, T.J., Rosenbach, A.S., Ideker, T., and Samson, L.D. (2004). Hot spots for modulating toxicity identified by genomic phenotyping and localization mapping. Mol. Cell *16*, 117–125.

Benton, M.G., Somasundaram, S., Glasner, J.D., and Palecek, S.P. (2006). Analyzing the dose-dependence of the Saccharomyces cerevisiae global transcriptional response to methyl methanesulfonate and ionizing radiation. BMC Genomics *7*, 305.

Burgis, N.E., and Samson, L.D. (2007). The protein degradation response of Saccharomyces cerevisiae to classical DNA-damaging agents. Chem. Res. Toxicol. *20*, 1843–1853.

Cairns, B.R., Lorch, Y., Li, Y., Zhang, M., Lacomis, L., Erdjument-Bromage, H., Tempst, P., Du, J., Laurent, B., and Kornberg, R.D. (1996). RSC, an essential, abundant chromatin-remodeling complex. Cell *87*, 1249–1260.

Cairns, B.R., Schlichter, A., Erdjument-Bromage, H., Tempst, P., Kornberg, R.D., and Winston, F. (1999). Two functionally distinct forms of the RSC nucleosome-remodeling complex, containing essential AT hook, BAH, and bromodomains. Mol. Cell *4*, 715–723.

Chai, B., Huang, J., Cairns, B.R., and Laurent, B.C. (2005). Distinct roles for the RSC and Swi/Snf ATP-dependent chromatin remodelers in DNA double-strand break repair. Genes Dev. *19*, 1656–1661.

Chambers, A.L., Brownlee, P.M., Durley, S.C., Beacham, T., Kent, N.A., and Downs, J.A. (2012). The two different isoforms of the RSC chromatin remodeling complex play distinct roles in DNA damage responses. PLoS ONE *7*, e32016.

Charles, G.M., Chen, C., Shih, S.C., Collins, S.R., Beltrao, P., Zhang, X., Sharma, T., Tan, S., Burlingame, A.L., Krogan, N.J., et al. (2011). Site-specific

acetylation mark on an essential chromatin-remodeling complex promotes resistance to replication stress. Proc. Natl. Acad. Sci. USA *108*, 10620–10625.

Chen, M., Licon, K., Otsuka, R., Pillus, L., and Ideker, T. (2013). Decoupling epigenetic and genetic effects through systematic analysis of gene position. Cell reports *3*, 128–137.

Cherry, J.M., Hong, E.L., Amundsen, C., Balakrishnan, R., Binkley, G., Chan, E.T., Christie, K.R., Costanzo, M.C., Dwight, S.S., Engel, S.R., et al. (2012). Saccharomyces Genome Database: the genomics resource of budding yeast. Nucleic Acids Res. *40* (Database issue), D700–D705.

Collins, S.R., Schuldiner, M., Krogan, N.J., and Weissman, J.S. (2006). A strategy for extracting and analyzing large-scale quantitative epistatic interaction data. Genome Biol. *7*, R63.

Collins, S.R., Kemmeren, P., Zhao, X.C., Greenblatt, J.F., Spencer, F., Holstege, F.C., Weissman, J.S., and Krogan, N.J. (2007). Toward a comprehensive atlas of the physical interactome of Saccharomyces cerevisiae. Mol. Cell. Proteomics *6*, 439–450.

Costanzo, M., Baryshnikova, A., Bellay, J., Kim, Y., Spear, E.D., Sevier, C.S., Ding, H., Koh, J.L., Toufighi, K., Mostafavi, S., et al. (2010). The genetic landscape of a cell. Science *327*, 425–431.

den Dulk, B., Sun, S.M., de Ruijter, M., Brandsma, J.A., and Brouwer, J. (2006). Rad33, a new factor involved in nucleotide excision repair in Saccharomyces cerevisiae. DNA Repair (Amst.) *5*, 683–692.

Frei, C., and Gasser, S.M. (2000). The yeast Sgs1p helicase acts upstream of Rad53p in the DNA replication checkpoint and colocalizes with Rad53p in S-phase-specific foci. Genes Dev. *14*, 81–96.

Gavin, A.C., Aloy, P., Grandi, P., Krause, R., Boesche, M., Marzioch, M., Rau, C., Jensen, L.J., Bastuck, S., Dümpelfeld, B., et al. (2006). Proteome survey reveals modularity of the yeast cell machinery. Nature *440*, 631–636.

Gong, F., Fahy, D., and Smerdon, M.J. (2006). Rad4-Rad23 interaction with SWI/SNF links ATP-dependent chromatin remodeling with nucleotide excision repair. Nat. Struct. Mol. Biol. *13*, 902–907.

Gong, F., Fahy, D., Liu, H., Wang, W., and Smerdon, M.J. (2008). Role of the mammalian SWI/SNF chromatin remodeling complex in the cellular response to UV damage. Cell Cycle *7*, 1067–1074.

Guénolé, A., Srivas, R., Vreeken, K., Wang, Z.Z., Wang, S., Krogan, N.J., Ideker, T., and van Attikum, H. (2013). Dissection of DNA damage responses using multiconditional genetic interaction maps. Mol. Cell *49*, 346–358.

Guzder, S.N., Sung, P., Prakash, L., and Prakash, S. (1993). Yeast DNA-repair gene RAD14 encodes a zinc metalloprotein with affinity for ultraviolet-damaged DNA. Proc. Natl. Acad. Sci. USA *90*, 5433–5437.

Hillenmeyer, M.E., Fung, E., Wildenhain, J., Pierce, S.E., Hoon, S., Lee, W., Proctor, M., St Onge, R.P., Tyers, M., Koller, D., et al. (2008). The chemical genomic portrait of yeast: uncovering a phenotype for all genes. Science *320*, 362–365.

Ideker, T., and Krogan, N.J. (2012). Differential network biology. Mol. Syst. Biol. *8*, 565.

Janićijević, A., Sugasawa, K., Shimizu, Y., Hanaoka, F., Wijgers, N., Djurica, M., Hoeijmakers, J.H., and Wyman, C. (2003). DNA bending by the human damage recognition complex XPC-HR23B. DNA Repair (Amst.) *2*, 325–336.

Jansen, L.E., Verhage, R.A., and Brouwer, J. (1998). Preferential binding of yeast Rad4.Rad23 complex to damaged DNA. J. Biol. Chem. *273*, 33111–33114.

Kent, N.A., Chambers, A.L., and Downs, J.A. (2007). Dual chromatin remodeling roles for RSC during DNA double strand break induction and repair at the yeast MAT locus. J. Biol. Chem. *282*, 27693–27701.

Krogan, N.J., Cagney, G., Yu, H., Zhong, G., Guo, X., Ignatchenko, A., Li, J., Pu, S., Datta, N., Tikuisis, A.P., et al. (2006). Global landscape of protein complexes in the yeast Saccharomyces cerevisiae. Nature *440*, 637–643.

Lenstra, T.L., Benschop, J.J., Kim, T., Schulze, J.M., Brabers, N.A., Margaritis, T., van de Pasch, L.A., van Heesch, S.A., Brok, M.O., Groot Koerkamp, M.J., et al. (2011). The specificity and topology of chromatin interaction pathways in yeast. Mol. Cell *42*, 536–549.

Luijsterburg, M.S., Lindh, M., Acs, K., Vrouwe, M.G., Pines, A., van Attikum, H., Mullenders, L.H., and Dantuma, N.P. (2012). DDB2 promotes chromatin decondensation at UV-induced DNA damage. J. Cell Biol. *197*, 267–281.

Min, J.H., and Pavletich, N.P. (2007). Recognition of DNA damage by the Rad4 nucleotide excision repair protein. Nature *449*, 570–575.

Niimi, A., Chambers, A.L., Downs, J.A., and Lehmann, A.R. (2012). A role for chromatin remodellers in replication of damaged DNA. Nucleic Acids Res. *40*, 7393–7403.

Pan, X., Yuan, D.S., Ooi, S.L., Wang, X., Sookhai-Mahadeo, S., Meluh, P., and Boeke, J.D. (2007). dSLAM analysis of genome-wide genetic interactions in Saccharomyces cerevisiae. Methods *41*, 206–221.

Pfaffl, M.W. (2001). A new mathematical model for relative quantification in real-time RT-PCR. Nucleic Acids Res. *29*, e45.

Prakash, S., and Prakash, L. (2000). Nucleotide excision repair in yeast. Mutat. Res. *451*, 13–24.

Prakash, S., Johnson, R.E., and Prakash, L. (2005). Eukaryotic translesion synthesis DNA polymerases: specificity of structure and function. Annu. Rev. Biochem. *74*, 317–353.

Rossio, V., Galati, E., Ferrari, M., Pellicioli, A., Sutani, T., Shirahige, K., Lucchini, G., and Piatti, S. (2010). The RSC chromatin-remodeling complex influences mitotic exit and adaptation to the spindle assembly checkpoint by controlling the Cdc14 phosphatase. J. Cell Biol. *191*, 981–997.

Saha, A., Wittmeyer, J., and Cairns, B.R. (2002). Chromatin remodeling by RSC involves ATP-dependent DNA translocation. Genes Dev. *16*, 2120–2134.

Saparbaev, M., Prakash, L., and Prakash, S. (1996). Requirement of mismatch repair genes MSH2 and MSH3 in the RAD1-RAD10 pathway of mitotic recombination in Saccharomyces cerevisiae. Genetics *142*, 727–736.

Sarkar, S., Kiely, R., and McHugh, P.J. (2010). The Ino80 chromatin-remodeling complex restores chromatin structure during UV DNA damage repair. J. Cell Biol. *191*, 1061–1068.

Schuldiner, M., Collins, S.R., Thompson, N.J., Denic, V., Bhamidipati, A., Punna, T., Ihmels, J., Andrews, B., Boone, C., Greenblatt, J.F., et al. (2005). Exploration of the function and organization of the yeast early secretory pathway through an epistatic miniarray profile. Cell *123*, 507–519.

Schuldiner, M., Collins, S.R., Weissman, J.S., and Krogan, N.J. (2006). Quantitative genetic analysis in Saccharomyces cerevisiae using epistatic miniarray profiles (E-MAPs) and its application to chromatin functions. Methods *40*, 344–352.

Sertic, S., Pizzi, S., Lazzaro, F., Plevani, P., and Muzi-Falconi, M. (2012). NER and DDR: classical music with new instruments. Cell Cycle *11*, 668–674.

Shannon, P., Markiel, A., Ozier, O., Baliga, N.S., Wang, J.T., Ramage, D., Amin, N., Schwikowski, B., and Ideker, T. (2003). Cytoscape: a software environment for integrated models of biomolecular interaction networks. Genome Res. *13*, 2498–2504.

Smerdon, M.J., and Lieberman, M.W. (1978). Nucleosome rearrangement in human chromatin during UV-induced DNA- reapir synthesis. Proc. Natl. Acad. Sci. USA *75*, 4238–4241.

Srivas, R., Hannum, G., Ruscheinski, J., Ono, K., Wang, P.L., Smoot, M., and Ideker, T. (2011). Assembling global maps of cellular function through integrative analysis of physical and genetic networks. Nat. Protoc. *6*, 1308–1323.

St Onge, R.P., Mani, R., Oh, J., Proctor, M., Fung, E., Davis, R.W., Nislow, C., Roth, F.P., and Giaever, G. (2007). Systematic pathway analysis using high-resolution fitness profiling of combinatorial gene deletions. Nat. Genet. *39*, 199–206.

Sugawara, N., Pâques, F., Colaiácovo, M., and Haber, J.E. (1997). Role of Saccharomyces cerevisiae Msh2 and Msh3 repair proteins in double-strand break-induced recombination. Proc. Natl. Acad. Sci. USA *94*, 9214–9219.

Teng, Y., Yu, Y., and Waters, R. (2002). The Saccharomyces cerevisiae histone acetyltransferase Gcn5 has a role in the photoreactivation and nucleotide excision repair of UV-induced cyclobutane pyrimidine dimers in the MFA2 gene. J. Mol. Biol. *316*, 489–499.

Timson, J. (1969). Hydroxyurea: comparison of cytotoxic and antimitotic activities against human lymphocytes in vitro. Br. J. Cancer *23*, 337–339.

Tong, A.H., and Boone, C. (2006). Synthetic genetic array analysis in Saccharomyces cerevisiae. Methods Mol. Biol. *313*, 171–192.

VanDemark, A.P., Kasten, M.M., Ferris, E., Heroux, A., Hill, C.P., and Cairns, B.R. (2007). Autoregulation of the rsc4 tandem bromodomain by gcn5 acetylation. Mol. Cell *27*, 817–828.

Verhage, R., Zeeman, A.M., de Groot, N., Gleig, F., Bang, D.D., van de Putte, P., and Brouwer, J. (1994). The RAD7 and RAD16 genes, which are essential for pyrimidine dimer removal from the silent mating type loci, are also required for repair of the nontranscribed strand of an active gene in Saccharomyces cerevisiae. Mol. Cell. Biol. *14*, 6135–6142.

Wade, S.L., Poorey, K., Bekiranov, S., and Auble, D.T. (2009). The Snf1 kinase and proteasome-associated Rad23 regulate UV-responsive gene expression. EMBO J. *28*, 2919–2931.

Yu, Y., Teng, Y., Liu, H., Reed, S.H., and Waters, R. (2005). UV irradiation stimulates histone acetylation and chromatin remodeling at a repressed yeast locus. Proc. Natl. Acad. Sci. USA *102*, 8650–8655.